Eur. Phys. J. E (2022) 45:21
https://doi.org/10.1140/epje/s10189-022-00174-6

THE EUROPEAN PHYSICAL JOURNAL E

Regular Article - Living Systems

Activity-driven phase separation and ordering kinetics of passive particles

Shambhavi Dikshit[a] and Shradha Mishra[b]

Department of Physics, Indian Institute of Technology (BHU), Varanasi 221005, India

Received 9 June 2021 / Accepted 14 February 2022 / Published online 7 March 2022

Abstract The steady state and phase ordering kinetics in a pure active Brownian particle system are studied in recent years. In binary mixture of active and passive Brownian particles passive particles are used as probe to understand the properties of active medium. In our present study, we study the mixture of passive and active Brownian particles. Here, we aim to understand the steady state and kinetics of small passive particles in the mixture. In our system, the passive particles are small in size and large in number, whereas ABPs are large in size and small in number. The system is studied on a two-dimensional substrate using overdamped Langevin dynamic simulation. The steady state and kinetics of passive particles are studied for various size and activity of active particles. Passive particles are purely athermal in nature and have dynamics only due to bigger ABPs. For small size ratio and activity, the passive particles remain homogeneous in the system, whereas on increasing size ratio and activity they form periodic hexagonal close pack (HCP) spanning clusters in the system. We have also studied the kinetics of growing passive particle clusters. The mass of the largest cluster shows a much slower growth kinetics in contrast to conserved growth kinetics in ABP system. Our study provides an understanding of steady state and kinetics of passive particles in the presence of bigger active particles. The mixture can be thought of as effect of big microorganism moving in passive medium.

1 Introduction

Collection of active Brownian particles (ABPs) undergoes a motility-induced phase separation (MIPS) without any cohesion at packing density much lower than the density for phase separation in corresponding passive systems [1–5]. Unlike for other active particle systems, where alignment interaction among the particle is responsible for the phase separation [6–9], the mechanism of phase separation in ABPs is due to the enhanced persistent motion of active particles [10,11].

Recent research have focussed the kinetics and steady state of pure ABPs or in the mixture of passive particles [12–16]. In a recent work of [17], a monodisperse mixture of active passive particles is studied for varying activity and packing fraction of ABPs, whereas in other studies a field theoretic approach is used to understand the propagation of active passive interface in the mixture of passive and active particles [18]. In the study of [19], a mixture of active passive particle is studied, and different phases and dynamics of system are studied. A variety of interesting properties and phases have been found when ABPs are placed in the mixture with passive particles. Asymmetric passive particles lead to directional transport and trapping when placed in the sea of ABPs [20–23]. Such systems can be useful in industrial and pharmaceutical applications. Symmetric passive particles in the mixture of ABPs have also been used as a probe to characterise the properties of ABPs [24–26]. Experiments on the dynamics of large passive beads in active bacterial fluid show the persistence motion of bead in bacterial solution [25]. In the binary mixture of ABPs with passive bead, large passive particles experience an effective attractive interaction analogous to depletion-induced attraction in asymmetric equilibrium binary mixture [5,26,27].

Most of the above studies of binary active-passive mixture are studied where passive particles are bigger in size and treated as a probe to characterise the properties of active medium [28–30] or monodisperse mixture of active passive particles and dynamics of different phases are explored [17–19]. Here, we ask the question, how the ABPs which are bigger in size can influence the characteristics of athermal passive particles ? The system resembles big microorganisms moving in passive fluid. In general, thermal and hydrodynamic effects are important in normal passive fluid, but we ignore it here to make the model simple and only study the effect of activity on the properties of passive particles.

[a] e-mail: shambhavidikshit.rs.phy18@itbhu.ac.in (corresponding author)
[b] e-mail: smishra.phy@iitbhu.ac.in

We consider a minimal model of mixture of small passive and big active Brownian particles on a two-dimensional substrate. Both types of particles interact through a short-range soft-repulsive interaction. The dynamics of active particles is driven by the active self-propulsion force and interaction with the particles in its surroundings, whereas passive particles can move only due to the interaction with other particles. The packing fraction of both particles are same and total packing fraction is kept fixed at 0.6. The dynamics and steady state of passive particles are studied for various size ratios of active and passive particles and dimensionless activity of ABPs.

Our main results are as follows: Starting from the random homogeneous mixture of active and passive particles, passive particles start to phase separate with time. The phase separation order parameter of passive particles grows with time and reaches a steady state with ~ 1 for large size ratio and activity and remains much lower than 1 for small size ratio and activity. Hence, a phase diagram is found in the plane of size ratio and activity. For moderate size ratio and activity, the clustered passive particles form hexagonal close-packed structures and start to overlap for large size ratio and activity. The cluster size distribution changes from exponential to power law and power converges to -2. Hence, passive particles form the spanning clusters [31] for larger size ratio and activity.

We further studied the kinetics of the phase separation. The mass of the largest cluster grows as a power law with time, with a much slower growth kinetics in contrast to conserved passive equilibrium and active systems [28,32–34]

The rest of the article is divided in the following manner. In Sect. 2, we describe the model in detail. Section 3 discusses the results of our study and finally in Sect. 6, we conclude our results.

2 Model

We consider a binary mixture of small athermal passive particles in the presence of large active Brownian particles (ABPs) on a two-dimensional substrate. The active and passive particles are modelled as discs of radius r_a and r_p, respectively. We choose $r_a > r_p$, active particles are larger in size compare to passive particles. The size ratio $S = \frac{r_a}{r_p}$ is one of the control parameters in the model. The radius of the passive particles is kept fixed and radius of active particles is tuned to vary the size ratio. We keep the packing fractions of both types of particles $\phi_a = \frac{\pi r_a^2 N_a}{L^2} = \phi_p = \frac{\pi r_p^2 N_p}{L^2} = 0.3$, hence the number of active particle N_a are less in comparison to that of passive particles N_p. Both active and passive particles are defined by their position $\mathbf{r}_i(t)$ and active particles are also having their orientation $\theta_i(t)$, which determines their direction of self-propulsion. They self-propel along their direction of orientation $\theta_i(t)$ with a constant self-propulsion speed v_0. The dynamical Langevin's equations of motion for position and orientation of active particles are

$$\frac{\mathrm{d}\mathbf{r}_i^a(t)}{\mathrm{d}t} = v_0\hat{\mathbf{n}}_i(t) + \mu\mathbf{F}_i(t) \tag{1}$$

where $\mathbf{n}_i(t) = (\cos(\theta_i(t)), \sin(\theta_i(t))$ is the unit direction of self-propulsion of ABP. The change in the orientation of the active particle is given by:

$$\frac{\mathrm{d}\theta_i}{\mathrm{d}t} = \sqrt{\nu_r}\eta_i(t) \tag{2}$$

here $\eta_i(t)$ is the random Gaussian white noise with mean zero and variance, $< \eta_i^r(t)\eta_j^r(t') >= \delta_{ij}\delta(t-t')$, where ν_r is the rotational diffusion constant of active particles. The equation of motion for the passive particle is given as:

$$\frac{\mathrm{d}\mathbf{r}_i^p(t)}{\mathrm{d}t} = \mu\mathbf{F}_i(t) \tag{3}$$

Here, the mobility, μ is chosen to be the same for both types of particles. $\mathbf{F}_i(t)$ is the force acting on the i^{th} particles, due to all other particles interacting with it

$$\mathbf{F}_i(t) = \sum_{j\neq i}\mathbf{F}_{ij}(t) \tag{4}$$

The force is obtained from the soft-repulsive pair potential $\mathbf{F}_{ij} = -\nabla U(r_{ij})$, where $U(r_{ij}) = K(r_{ij} - (r_{\alpha i} + r_{\alpha' j}))^2$ if $r_{ij} \leq (r_{\alpha i} + r_{\alpha' j})$ and 0 otherwise. r_{ij}=$|r_i$ - $r_j|$ and K is the force constant and r_α, is the radius of active or passive particles for α and α'= a or p, respectively. ν_r^{-1} is the time scale over which the orientation of an active particle changes. Hence, $l_p = v_0\nu_r^{-1}$, is the persistence length or run length, is the typical distance travelled by an active particle before it changes its direction. In our study, $l_p = (100r_p$ to $600r_p)$ is tuned by tuning SPPs v_0. The $(\mu K)^{-1} = 0.7$ defines the elastic time scale in the system. We define the dimensionless activity $\bar{v} = \frac{l_p}{r_p}$ as the ratio of persistent length to the size of passive particles. The size ratio S and $\bar{v}$ are the two tuning parameters in the model. A schematic cartoon of system is shown in Fig. 1, where red big particles are ABPs and small grey particles are passive. The white dots on red particles represent their instantaneous direction of orientation θ.

We start with random non-overlapping arrangement of active and passive particles on a two-dimensional square substrate of linear dimension $L = 250r_p$ with periodic boundary condition. Eqs. (1)–(3) are updated and one simulation step is counted after updation of all the particles once. The time step $\tau = 5\times10^{-4}$ and total 6×10^4 simulation steps are used to get the results. We have used 20 independent realisations to get averaged data and different realisations are obtained by initialising the system with the similar initial conditions but different configurations.

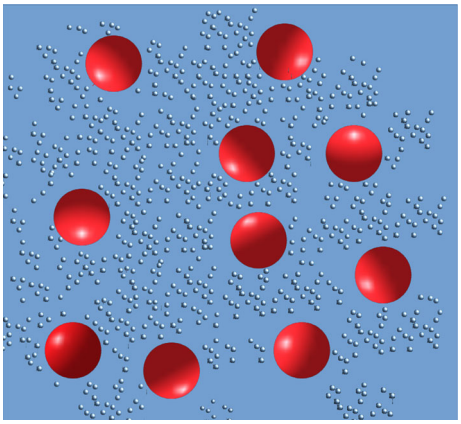

Fig. 1 (Color online) Schematic diagram of the model. It shows the initial homogeneous state of the system. Here, the colours and sizes represent two types of particles. Bigger particles (red) are active particles and smaller particles (grey) are passive particles. Small white dot on red particles denote the instantaneous orientation direction θ of ABPs

We first characterise the effect of size ratio and activity on the steady state of the athermal passive particles in the mixture. Then, we study the kinetics to the steady state.

3 Results

We start with the random homogeneous distribution of active and passive particles and Eqs. (1)–(3) are integrated to update the position and orientation of active and position of passive particles. In Fig. 2, we plot the time evaluation snapshot of local density of passive particles at different times = 0.05, 0.5 and 30.0 and for two different size ratios $S = 10$ and 6 and for $\bar{v} =$ 100, 300 and 600. The bright and dark regions show the lower and higher local density of passive particles, respectively. Local density ρ_p is defined as: *the number of passive particles in the small coarse-grained area* ($a = 5r_p \times 5r_p$). In Fig. 2(h-i), we plot the probability distribution function (PDF) of local density $P(\rho_p)$ for the same parameters as in Fig. 2a–f. The tail of the distribution is larger for large size ratio $S = 10$ and activity $\bar{v} = 600$. As time progresses, the passive particle starts to come close to each other. Hence, local density ρ_p of passive particle rich region grows or passive particles phase separate. To characterise the phase separation, we calculate the phase separation order parameter *(PSOP)*,$\phi(t)$. The analogy of *(PSOP)* comes from standard liquid gas phase separation [35]. Using the same analogy, in our system we define *(PSOP)*, as $\phi(t) =< (n_p(t) - n_a(t))/(n_p(t) + n_a(t)) >$, where $n_p(t)$ and $n_a(t)$ are calculated as the number of active and passive neighbouring particles around a passive particle. $< .. >$ means average over all passive particles and 20 independent realisations. With the above definition if passive particles are mainly surrounded by passive particles then the $\phi(t)$ will be close to 1 and if, found in the mixture of active and passive, then it will be close to 0.

With time $\phi(t)$ grows and approaches a steady state, we calculate the steady state $\phi =< \phi(t) >_t$, where $< .. >_t$ is the average of $\phi(t)$ over a time interval in the steady state. In Fig. 2g, we plot the phase diagram in the plane of activity and size ratio $(S, \bar{v})$. The colour shows the magnitude of *PSOP*, $\phi(t)$. For large activity and size ratio, phase separation increases in the system.

4 Characteristics of steady state

4.1 Radial distribution function (RDF) $g_{pp}(r)$

As discussed in previous section, system shows the phase separation for larger size ratio and activity. Hence, clustering increases with increasing S and $\bar{v}$. We further characterise the structure of the clusters by calculating the radial distribution function *(RDF)* of passive–passive particles for different size ratio S and $\bar{v}$. The *RDF*, $g_{pp}(r)$ gives the probability of finding a passive particle at a radial distance r from the centre of the given passive particle. In Fig. 3, we plot the $g_{pp}(r)$ *vs.* scaled distance r/r_p, for passive–passive particles for three different activities $\bar{v} = 100$, 300 and 600 and varying the size ratio $S = 6$, 8 and 10. For small activity and $S = 6$ as shown in Fig. 3a, the first peak appears at $r/r_p \approx 2$ and second peak is at 4 and few more higher order peaks are present. But as we increase $S > 8$, the location of first peak remains almost the same but a small hump in second peak appears at $r/r_p = 2\sqrt{3}$, which is due to the presence of hexagonal close packed structure (HCP) in the clusters. Also for $S > 6$, higher order peaks are more pronounced. The zoom in plot in Fig. 3a (inset) shows the enlarged second peak for three $S = 6$, 8 and 10. As we increase, $\bar{v} = 300$, the location of the first peak shifts at distance smaller than $r/r_p \approx 2$, which suggests overlapping particles due to soft-repulsive interaction. The second peak of $g_{pp}(r)$ appears at $r/r_p \approx 2\sqrt{3}$, for size ratio $S > 6$, hence HCP structure of clusters. Also the distinct higher order peaks are found for larger size ratio $S > 8$. Again the inset Fig. 3b shows the zoom in second peak of the $g_{pp}(r)$. On further increasing $\bar{v} = 600$, the first and second peak of $g_{pp}(r)$, systematically shifts towards the small scaled distance, hence more overlapping particle clusters, the distinct nature of higher order peaks decreases on increasing S. As we increase S and activity, the passive particles start to overlap and it leads to weaker periodic clusters as shown in the inset Fig. 3c.

The figure shows the zoom in second peak, where the structure in second peak has been disappeared for large activity $\bar{v} = 600$. In the bottom panel of Fig. 3d–f we show the zoom in structure of particle clusters for $\bar{v} = 300$ for size ratios $S = 6$, 8 and 10, respectively. As it is very clear that for this intermediate activity

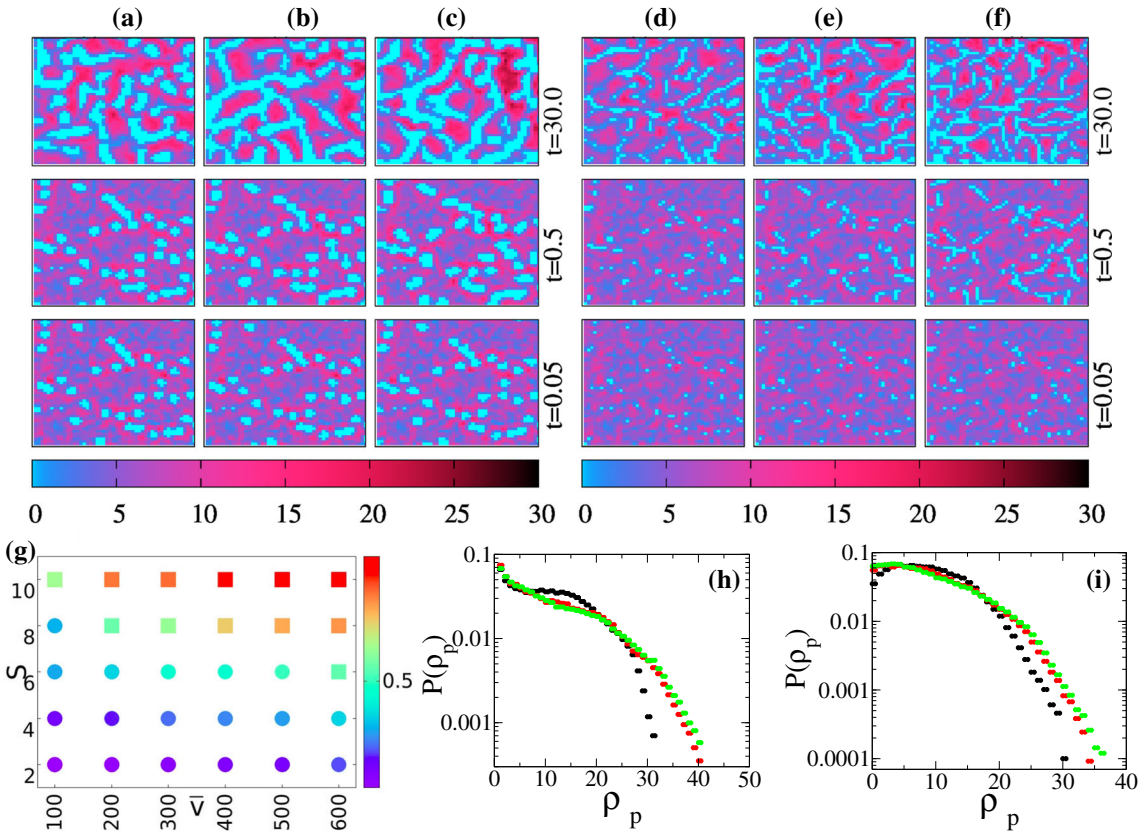

Fig. 2 (Color online) The real space snapshots of local density of passive particles at different times. **a**–**c** are for size ratio 10 and $\bar{v}$= 100, 300 and 600, respectively. **d**–**f** are for size ratio 6 and $\bar{v}$= 100, 300 and 600, respectively. From bottom to top panels are for times, $t = 0.05$, $t = 0.5$ and $t = 30.0$. The colour bar shows the local density of passive particles. **g** The lower colour plot shows the phase separation order parameter *(PSOP)* in the plane of size ratio and activity $(S, \bar{v})$. **h**–**i** Probability distribution function (PDF) of local density of passive particles $P(\rho_p)$ is plotted for two different size ratios 10 and 6 ((h) and (i)), respectively, and for three $\bar{v}$= 100, 300 and 600

$\bar{v} = 300$ (Fig. 3b) as we increase S the periodicity within the cluster increases.

Hence, using *RDF*, we find the periodic *HCP* nature of particle clusters first increases on increasing activity and size ratio and again for very large $\bar{v} = 600$ and $S = 10$, overlapping large clusters. Now, we further characterise the characteristics of large clusters by calculating the cluster size distribution *(CSD)* of different size clusters.

4.2 Cluster size distribution (CSD)

To further understand the characteristics of clusters, we calculate the probability distribution function of different sized clusters. A cluster is defined as set of particles connected by a distance smaller or equal to $2r_p$ *(diameter of the particle)*. A cluster of size n has n *−particles connected cluster*. Then, we calculate the number of different sized cluster in the total system. In this manner, all particles are part of a single particle cluster. Hence, number of clusters of size $n = 1$ is total number of particles [5]. We further calculate the fraction of cluster of size n, or cluster size distribution *(CSD)*. In Fig. 4, we plot the normalised cluster size distribution *(CSD)* $P(n)/P(1)$, where $P(i)$ is obtained from the counting all the clusters of size $i = 1, 2, ..., n$. In Fig. 4a, we plot the *CSD* for activity $\bar{v} = 100$ for three different size ratios $S = 6$, 8 and 10. For small activity, $\bar{v} < 300$ and size ratio $S < 8$, the *CSD* decay exponentially at $n > 20$. Hence, for small activity and size ratio, we find small clusters and particles are well separated from each other (as shown in Fig. 4b). Hence, weak clusters as found in the *RDF*, $g_{pp}(r)$ plot as shown in Fig. 3a. As we increase size ratio $S > 6$, for $\bar{v} = 100$, clustering increases and *CSD* decay as a power law. The power approaches -2.5 for large size ratio $S = 10$. The real space snapshots of particles show the enhanced clustering on increasing S. For moderate activity $\bar{v} = 300$, *CSD* for small size ratio $S = 6$, is exponential with large exponential tail and for large size ratio $S > 6$, the exponential tail approaches to power law tail -2. Also the real space snapshots show the clustering increases on increasing S. But for larger size ratio $S = 10$, particles start to overlap and HCP structure weakens as shown in Fig. 3b. As we further increase activity $\bar{v} = 600$, the *CSD* is power law for all size ratios $S = 6$, 8 and 10 and power slowly converges to -2 for largest size ratio 10. The power -2 suggests that for large activity pas-

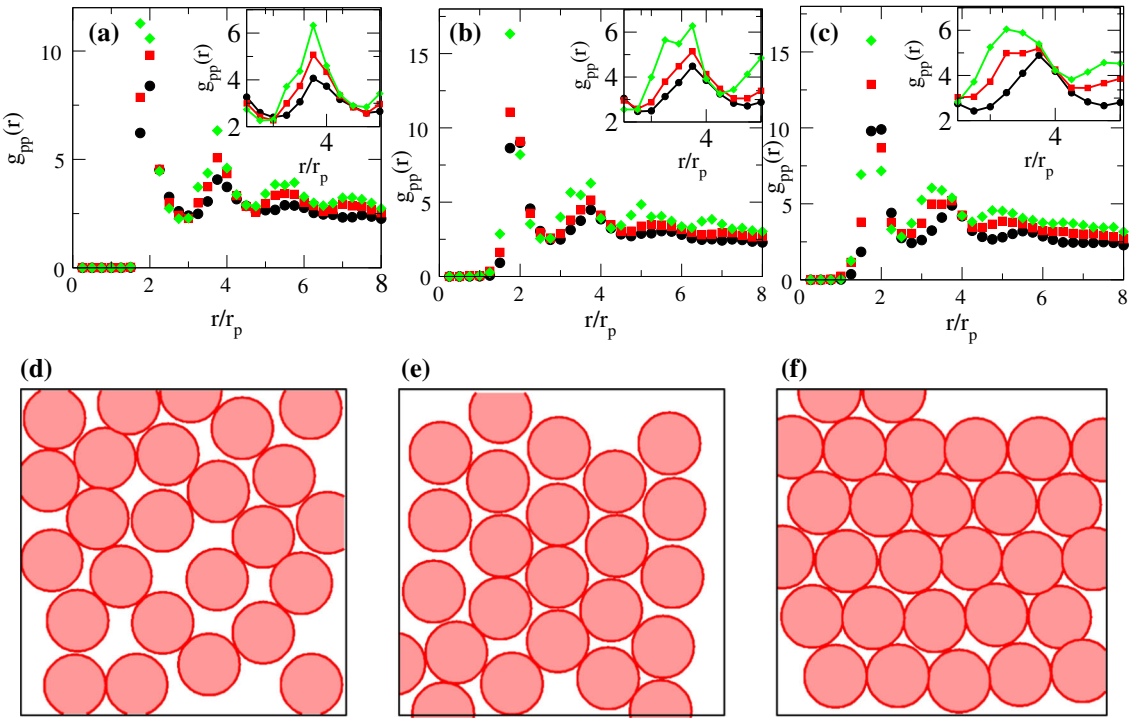

Fig. 3 (Color online) Passive–passive radial distribution function *(RDF)*, $g_{pp}(r)$ is plotted for different parameters. **a**–**c** is for fixed activity and varying size ratio. $\bar{v}$ is varied for three different values, 100, 300 and 600. **a** is for $\bar{v} = 100$ **b** is for $\bar{v} = 300$ and **c** is for $\bar{v} = 600$ and size ratio S is taken 6, 8 and 10 for black ○, red □ and green ⋄, respectively. Inset figures are zoomed for the same parameters as mentioned in (a), (b) and (c). At the bottom **d**, **e** and **f** are real space (zoomed) snapshots to support the cluster formation by fixing the activity $\bar{v} = 300$ and $t = 30$ for size ratios 6, 8 and 10, respectively

sive particles form the percolating clusters spanning the whole system [31].

5 Growth kinetics

After understanding the steady state properties of the mixture, we study the kinetics of phase separation of athermal passive particles. We study the kinetics of growing cluster by calculating the mass of the largest cluster at different times, $< m(t) >$.

In Fig. 5, we plot the $< m(t) >$ for two different size ratios $S = 10$ and 6 and for different $\bar{v}$. where $< .. >$ is mean over 50 independent realisations. In Fig. 5a, we plot $< m(t) >$ for size ratio 10 for three different activities $\bar{v} = 100, 300$ and 600. For all activities and $S = 10$, at very early time $t < 10^{-2}$, $< m(t) >$ grows with time and then for an intermediate times t $(10^{-2}, 10)$, growth becomes slow and $< m(t) >$ develops a plateau and again starts to grow for late times $t \geq 10$. The plateaus region decreases with increasing activity since activity is enhancing the clustering in passive particles. The only mechanism of motion of passive particles is due to the interaction of them with other passive and active particles. For small activity and size ratio, active particles have lesser probability to interact with passive particles, hence slower dynamics of passive particles. This led them to stuck for some intermediate times. At late times, they do experience the effect of active particles and show the enhanced motion and hence clustering. This is the reason for the decrease in the plateaus region for larger activity and size ratio. For $S = 6$ and small $\bar{v} = 100$, the very early time $(t \simeq 0.001 - 0.02)$, when the initial configuration equilibrate, dynamics is fast and hence the $< m(t) >$ grows with time. Then, particles are stuck in regions with not many active particles in their surroundings hence slow dynamics and we experience plateaus region for intermediate time $(t \simeq 0.02 - 10)$ Fig. 5c–d. Then, they further get more interaction with active particles and $< m(t) >$ grow as $t^{1/3}$ with time for late time $(t \simeq 10 - 100)$ Fig. 5e–f. After time $t \simeq 90$ the $< m(t) >$ shows saturation due to finite system size. Increasing the activity leads the passive particles to spend less time in intermediate time region and so the size of plateau decreases with increasing activity. The late time growth of $< m(t) > \sim t^{1/3}$ for all activities. In Fig. 5(right panel), we show the plot of $< m(t) >$ for size ratio $S = 6$. The growth of $< m(t) >$ shows the same behaviour as for $S = 10$ Fig. 5(right panel), only the plateaus region is increased for $S = 6$. For largest activity $\bar{v}$ and size ratio $S = 10$, $< m(t) >$ increases monotonically with time t with $< m(t) > \sim t^{1/3}$.

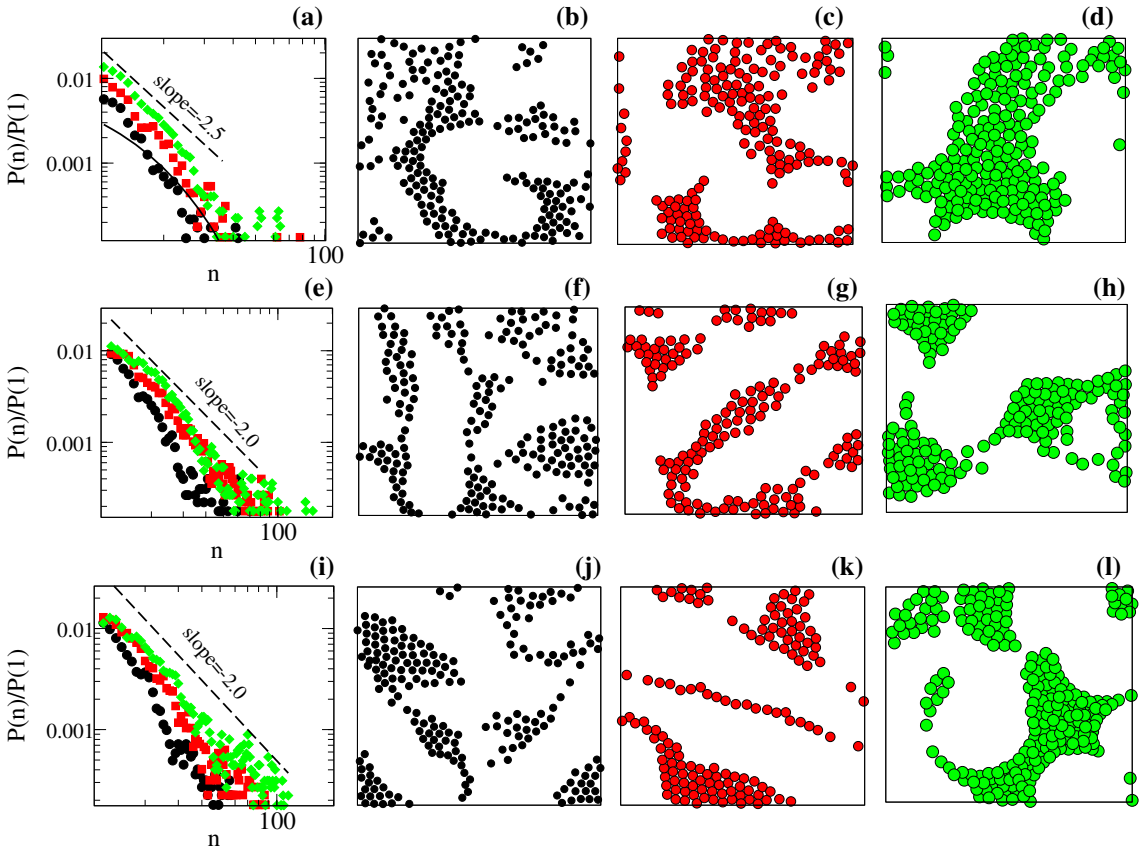

Fig. 4 (Color online) Cluster size distribution *(CSD)* and real space snapshots of part of the system are plotted for different parameters. Different panels **a**–**d** are for fixed $\bar{v} = 100$, **e**–**h** are for $\bar{v} = 300$ and **i**–**l** are for $\bar{v} = 600$ and black, red and green colours are for size ratios 6, 8 and 10, respectively. *CSD* is shown in (a),(e) and (i) for $\bar{v} = 100, 300$ and 600, respectively, and for size ratio 6, 8 and 10. Symbols have the same meaning as in Fig. 3

6 Conclusion

We have studied the phase separation and ordering kinetics of a binary mixture of passive and active Brownian particles on a two-dimensional substrate with periodic boundary condition. The passive particles are smaller in size in comparison to the ABPs. The ABP moves along the direction of their heading and both types of particles interact through a short-range soft-core repulsive interaction. Hence, the dynamics of passive particles are only due to interaction force among the particles. The system is studied for various size ratios S and activities $\bar{v}$ of active particles. We focus our study on the steady state and kinetics of small passive particles in the presence of big passive particles. Starting from the random homogeneous state, the clustering of small passive particle is measured by calculating phase separation order parameter *(PSOP)*. The *PSOP* is small for size ratio $S < 6$ and small activity $\bar{v} < 300$, whereas for large size ratio $S > 8$ and higher activity $\bar{v} > 300$, *PSOP* approaches ~ 1. The clusters of passive particles are random small clusters for small size ratio and activity and HCP structures are formed for intermediate size ratio $S = 8$ and activity $\bar{v} = 300$ and then overlapping clusters are found for large size ratio and activity $S > 8$ and $\bar{v} = 300$. The Cluster size distribution decays exponentially for small size ratio and activity and approaches to a power law decay with exponent -2 for large size ratio and activity. The power law decay with power -2 indicates the formation of connected clusters as in [31] for large size ratios and activities.

We have also calculated the kinetics of growing cluster of passive particles. The mean mass of the largest cluster grows with time as a power law. The growth law is much smaller than the conserved growth kinetics of corresponding equilibrium and active Brownian systems [33,34,36–38].

Hence, our study gives the steady state of collection of passive particles moving under the effect of dynamics of active Brownian particle. It focuses on the steady state and kinetics for binary mixture where passive particles are much smaller than the ABPs. The system resembles the effect of big microorganism moving in passive medium.

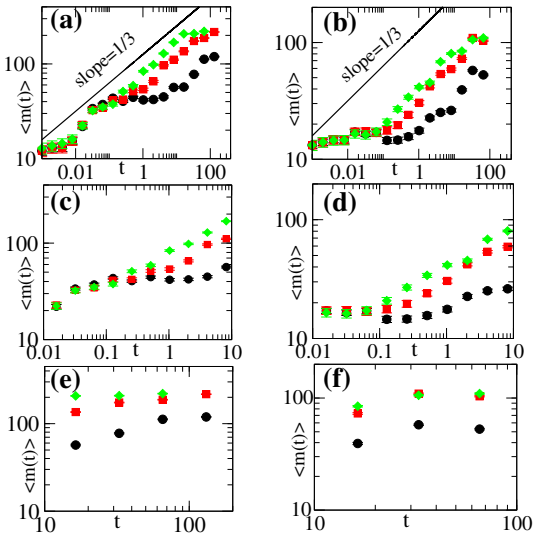

Fig. 5 (Color online) Mean mass of the largest cluster $< m(t) >$ is plotted for activities $\bar{v} = 100, 300$ and 600. Left panel is for size ratio 10 and right panel is for size ratio 6. Black, red and green show the activities 100, 300 and 600, respectively. Straight line is the line with slope 1/3. **c**, **d** and **e**, **f** are the zoomed plot for intermediate ($t \simeq 0.01 - 10$) and late time ($t \simeq 10 - 100$) region for the same parameters

Acknowledgements The support and the resources provided by PARAM Shivay Facility under the National Supercomputing Mission, Government of India at the Indian Institute of Technology, Varanasi, are gratefully acknowledged. Computing facility at Indian Institute of Technology(BHU), Varanasi, is gratefully acknowledged.

Declarations

Conflicts of interest There are no conflicts of interest to declare.

Contribution of authors SM initiated the project, SD performed the numerical simulation, analysed the results and both the authors have equally contributed in writing the manuscript.

References

1. S. Ramaswamy, Annu. Rev. Condens. Matter. Phys. **1**, 323 (2010)
2. M.C. Marchetti, J.F. Joanny, S. Ramaswamy, T.B. Liverpool, J. Prost, M. Rao, R.A. Simha, Rev. Mod. Phys. **85**, 1143 (2013)
3. P. Romanczuk, M. Bär, W. Ebeling, B. Lindner, L. Schimansky-Geier, Eur. Phys. J. ST **1**, 202 (2012)
4. C. Bechinger, R.D. Leonardo, H. Lowen, C. Reichhardt, G. Volpe, G. Volpe, Rev. Mod. Phys. **88**, 045006 (2016)
5. P. Dolai, A. Simha, S. Mishra, Soft Matter **14**, 6137 (2018)
6. T. Vicsek, A. Czirok, E. Ben-Jacob, I. Cohen, O. Shochet, Phys. Rev. Lett. **75**, 1226 (1995)
7. C. Bechinger, R. Di Leonardo, H. Lowen, C. Reichhardt, G. Volpe, G. Volpe, Rev. Mod. Phys., **88** (2016)
8. H. Chate, F. Ginelli, G. Gregoire, F. Raynaud, Phys. Rev. E. **77**, 046113 (2008)
9. J.P. Singh, S. Mishra, Physica A **544**, 123530 (2020)
10. M.E. Cates, J. Tailleur, Annu. Rev. Condens. Matter. Phys. **6**, 219 (2015)
11. F. Alaimo, A. Voigt, Phys. Rev. E. **98**, 032605 (2018)
12. F. Kümmel, P. Shabestari, C. Lozano, G. Volpe, C. Bechinger, Soft Matter. **11**, 6187 (2015)
13. L. Angelani, C. Maggi, M.L. Bernardini, A. Rizzo, R. Di Leonardo, Phys. Rev. Lett. **107**, 138302 (2011)
14. R. Di Leonardo, L. Angelani, D. Dell'Arciprete, G. Ruocco, V. Iebba, S. Schippa, M.P. Conte, F. Mecarini, F. De Angelis, E. Di Fabrizio, PNAS **107**(21), 9541 (2010)
15. D. Ray, C. Reichhardt, C.J. Olson Reichhardt, Phys. Rev. E. **70**, 013019 (2014)
16. J.P. Singh, S. Mishra, Physica A. **544**, 123530 (2020)
17. J. Stenhammar, R. Wittkowski, D. Marenduzzo, M.E. Cates, Phys. Rev. Lett. **114**, 018301 (2015)
18. A. Wysocki, R.G. Winkler, G. Gompper, New J. Phys. **18**, 123030 (2016)
19. R. Wittkowski, J. Stenhammar, M.E. Cates, New J. Phys. **19**, 105003 (2017)
20. S. Pattanayak, R. Das, M. Kumar, S. Mishra, Eur. Phys. J. E **42**, 62 (2019)
21. P. Malgaretti, H. Stark, J. Chem. Phys. **146**, 174901 (2017)
22. C. Reichhardt, C.J. Olson Reichhardt, Phys. Rev. E. **97**, 052613 (2018)
23. I. Buttinoni, J. Bialké, F. Kümmel, H. Löwen, C. Bechinger, T. Speck, Phys. Rev. Lett. **110**, 238301 (2013)
24. C.P. Beatrici, R.M.C. de Almeida, L.G. Brunnet, Phys. Rev. E. **95**, 032402 (2017)
25. X.-L. Wu, A. Libchaber, Phys. Rev. Lett. **84**, (1999)
26. A.E. Patteson, A. Gopinath, P.K. Purohit, P.E. Arratia, Soft Matter. **12**, 2365 (2016)
27. P. Liu, S. Ye, F. Ye, K. Chen, M. Yang, Phys. Rev. Lett. **124**, 158001 (2020)
28. R. Ni, M.A. Cohen Stuart, M. Dijkstra, Nature Communi. **4**, 2704 (2013)
29. R. Ni, M.A.C. Stuart, M. Dijkstra, P.G. Bolhuis, Soft Matter. **10**, 6609 (2014)
30. F. Kümmel, P. Shabestari, C. Lozano, G. Volpe cd, C. Bechinger, Soft Matter. **11**, 6187 (2015)
31. D.C. Rapaport, J. Stat. Phys. **66**, 679 (1992)
32. S. Puri, V. Wadhawan (eds.), *Kinetics of phase transition* (CRC Press, Boac Raton, 2009)
33. S. Pattanayak, S. Mishra, S. Puri, Phys. Rev. E. **104**, 014606 (2021)
34. S. Pattanayak, S. Mishra, S. Puri, Soft Mater. (2021)
35. R. K. Pathria, Stat. Mech. (1972)
36. J. Stenhammar, A. Tiribocchi, R.J. Allen, D. Marenduzzo, M.E. Cates, Phys. Rev. Lett. **111**, 145702 (2013)
37. R. Wittkowski, A. Tiribocchi, J. Stenhammar, R.J. Allen, D. Marenduzzo, M.E. Cates, ncomms **5351** (2014)
38. Theory of phase-ordering kinetics, A.J. Bray, Adv. Phys., **43**, (1994)